AGU PUBLICATIONS

Geophysical Research Letters

RESEARCH LETTER
10.1002/2017GL074665

Key Points:
- Aerosol organic concentrations were enhanced by multiday accumulation of isoprene-related secondary particle mass
- Three types of single-particle composition had mass fragments similar to three mass-weighted aerosol mass spectrometer composition factors
- Isoprene-related organic aerosol mass fragments were mostly found on sulfate-containing particles, indicating selective uptake to particles

Supporting Information:
- Supporting Information S1

Correspondence to:
L. M. Russell,
lmrussell@ucsd.edu

Citation:
Liu, J., L. M. Russell, A. K. Y. Lee, K. A. McKinney, J. D. Surratt, and P. J. Ziemann (2017), Observational evidence for pollution-influenced selective uptake contributing to biogenic secondary organic aerosols in the southeastern U.S., *Geophys. Res. Lett.*, *44*, 8056–8064, doi:10.1002/2017GL074665.

Received 13 MAR 2017
Accepted 24 JUL 2017
Accepted article online 28 JUL 2017
Published online 13 AUG 2017

Observational evidence for pollution-influenced selective uptake contributing to biogenic secondary organic aerosols in the southeastern U.S.

J. Liu[1], L. M. Russell[1], A. K. Y. Lee[2], K. A. McKinney[3], J. D. Surratt[4], and P. J. Ziemann[5]

[1]Scripps Institution of Oceanography, University of California, San Diego, La Jolla, California, USA, [2]Department of Civil and Environmental Engineering, National University of Singapore, Singapore, [3]School of Engineering and Applied Sciences, Harvard University, Cambridge, Massachusetts, USA, [4]Department of Environmental Sciences and Engineering, Gillings School of Global Public Health, University of North Carolina at Chapel Hill, Chapel Hill, North Carolina, USA, [5]Department of Chemistry and Biochemistry and at the Cooperative Institute for Research in Environmental Sciences, University of Colorado Boulder, Boulder, Colorado, USA

Abstract During the 2013 Southern Oxidant and Aerosol Study, aerosol mass spectrometer measurements of submicron mass and single particles were taken at Look Rock, Tennessee. Their concentrations increased during multiday stagnation events characterized by low wind, little rain, and increased daytime isoprene emissions. Organic mass (OM) sources were apportioned as 42% "vehicle-related" and 54% biogenic secondary organic aerosol (bSOA), with the latter including "sulfate-related bSOA" that correlated to sulfate ($r = 0.72$) and "nitrate-related bSOA" that correlated to nitrate ($r = 0.65$). Single-particle mass spectra showed three composition types that corresponded to the mass-based factors with spectra cosine similarity of 0.93 and time series correlations of $r > 0.4$. The vehicle-related OM with *m/z* 44 was correlated to black carbon, "sulfate-related bSOA" was on particles with high sulfate, and "nitrate-related bSOA" was on all particles. The similarity of the *m/z* spectra (cosine similarity = 0.97) and the time series correlation ($r = 0.80$) of the "sulfate-related bSOA" to the sulfate-containing single-particle type provide evidence for particle composition contributing to selective uptake of isoprene oxidation products onto particles that contain sulfate from power plants.

1. Introduction

Organic compounds contribute the largest fraction of submicron aerosol mass in many regions worldwide, and secondary organic aerosols (SOA) contribute as much as 70% of the organic carbon mass (OM) in aerosol particles [*Hallquist et al.*, 2009]. Emission rates of both isoprene and monoterpenes in the southeastern United States [*Goldstein et al.*, 2009] compete with the rates measured in tropical rain forests [*Rinne et al.*, 2002]. One reason that mean annual temperatures in the southeastern United States decreased in the twentieth century despite overall global-mean warming may be the direct radiative effect of the SOA formed from biogenic volatile organic compounds, known as bSOA [*Goldstein et al.*, 2009; *Portmann et al.*, 2009]. This recent cooling trend may also have contributions from internal variability [*Banerjee et al.*, 2017], aerosol sources aloft [*Ford and Heald*, 2013], cloud forcing [*Yu et al.*, 2014], particle phase water [*Nguyen et al.*, 2016], and other changes in particle composition [*Kim et al.*, 2015]. The high global flux of biogenic volatile organic compounds of 1000 Tg yr^{-1} [*Guenther et al.*, 2012] provides ample precursors that may form bSOA in many regions of the world.

Identifying the contributions of different natural and man-made emission sources to SOA quantifies the factors that control bSOA. Data inversion methods have been applied to aerosol mass spectrometry (AMS) measurements to separate and quantify different types or "factors" of bSOA in aerosol OM with both reasonable accuracy and consistency [*Budisulistiorini et al.*, 2013, 2015; *Chen et al.*, 2015; *Corrigan et al.*, 2013; *Robinson et al.*, 2011; *Slowik et al.*, 2011; *Xu et al.*, 2015b]. Two biogenic factors in particular have been identified at multiple locations and shown to have similar chemical compositions (spectra of mass fragments) and correlations [*Devore and Berk*, 2012] to tracers: one factor with high *m/z* 82 (which we refer to as Factor82, also referred to as 82fac, IEPOX OA, or Isoprene OA, as noted in Table S4) [*Budisulistiorini et al.*, 2013, 2015; *Chen et al.*, 2015; *Robinson et al.*, 2011; *Slowik et al.*, 2011; *Xu et al.*, 2015b] showed moderate to strong ($r = 0.7$ to 0.88) correlations to sulfate [*Budisulistiorini et al.*, 2013, 2015; *Xu et al.*, 2015b] and another factor with a

characteristic fragment ion at *m/z* 91 (which we refer to as Factor91, also referred to as 91fac, OOA3, bSOA1, bSOA2, or Isoprene OA as noted in Table S4) [*Budisulistiorini et al.*, 2015; *Chen et al.*, 2015; *Lee et al.*, 2016b; *Robinson et al.*, 2011]. The consistent identification of these two factors in studies across North and South America as well as Europe indicates both the prevalence of bSOA worldwide and the general similarity of their composition (Table S4).

These similarities in bSOA chemical composition suggest commonalities in their atmospheric formation processes, for which chamber studies provide a proxy. Recent studies have provided a link between chamber-generated and atmospheric isoprene-related bSOA by identifying the characteristic fragment ion at *m/z* 82 found in AMS data sets to be associated with isomeric isoprene epoxydiols (IEPOX)-derived SOA [*Budisulistiorini et al.*, 2013; *Lin et al.*, 2012]. To understand what factors contribute to forming this IEPOX-derived bSOA, chamber studies have investigated a variety of different atmospheric conditions: particle acidity [*Gaston et al.*, 2014b; *Surratt et al.*, 2010] and particle-phase water [*Nguyen et al.*, 2011, 2015; *H. Zhang et al.*, 2011] were both found to increase IEPOX-related bSOA. The source of the other bSOA (Factor91) is less clear but is likely associated (in part) with gas-phase isoprene oxidation pathways that do not involve particle-phase reactions such as low-volatility multifunctional hydroperoxides produced from oxidation of isoprene hydroxyhydroperoxides [*Budisulistiorini et al.*, 2016; *Krechmer et al.*, 2015; *Liu et al.*, 2016; *Riva et al.*, 2016]. A high *m/z* 91 signal was measured in chamber studies of reactions of β-pinene and NO_3 radical [*Boyd et al.*, 2015] and of ozonolysis of β-caryophyllene [*Chen et al.*, 2015], suggesting that *m/z* 91 could be an indicator for bSOA formed from monoterpene or sesquiterpene oxidation in ambient aerosol mass spectra [*Boyd et al.*, 2015].

Atmospheric bSOA measurements have not found a correlation between IEPOX-related bSOA and either calculated particle-phase water or acidity [*Budisulistiorini et al.*, 2015; *Rattanavaraha et al.*, 2016; *Worton et al.*, 2013; *Xu et al.*, 2015b], but other atmospheric factors could have hidden such relationships because of larger variability in other field conditions. *Xu et al.* [2016] showed that in sulfate-rich plumes, sulfate enhances the heterogeneous reaction rates of IEPOX due to both enhanced particle surface area and particle acidity. *Hu et al.* [2016] used the similarity in the mass size distribution peak of the characteristic *m/z* 82 fragment ion and sulfate in particles from both the southeastern U.S. and the Amazon to suggest sulfate control of the IEPOX uptake formation pathway. Both studies provide indirect evidence of contributions to bSOA from heterogeneous reactions of IEPOX with sulfate based on correlations of tracers and submicron mass composition.

To provide more direct evidence of the processes controlling bSOA formation, we compared characteristic fragment ions associated with bSOA identified in submicron particle mass and in single particles measured during the 2013 Southern Oxidant and Aerosol Study (SOAS) at Look Rock, Tennessee. The prevalence of biogenic emissions and the meteorological conditions resulted in large contributions of bSOA to OM. Single-particle AMS measurements with light scattering (LS) provided direct information on differences in particle composition. As a result, this work provides biogenic-specific single-particle spectra to evaluate the role of particle composition-dependent processes in SOA formation.

2. Measurements

As part of the SOAS campaign from 1 June to 17 July 2013 in a forested area at Look Rock, Tennessee, we measured size-resolved nonrefractory chemical composition of submicron particles with a high-resolution time-of-flight aerosol mass spectrometer (AMS, Aerodyne Research, Inc.). The LS module attached to the AMS triggered collection of single-particle nonrefractory mass fragment ion spectra for particles in the vacuum aerodynamic diameter range of 350 to 700 nm (i.e., mobility diameter of 230 to 500 nm, using 5% sampling efficiency as the cutoff diameters; see Text S3) [*Cross et al.*, 2007, 2009; *Kostenidou et al.*, 2007]. The same aerosol inlet [*Bates et al.*, 2012] was used for filter collection for Fourier transform infrared (FTIR) spectroscopy [*Russell et al.*, 2009; *Takahama et al.*, 2013] and particle size distributions by Scanning Electrical Mobility Spectrometer (SEMS, Model 2000C, Brechtel Manufacturing Incorporated). Specific details of instrument operation, performance, and calibration, including evaluation of the AMS collection efficiency (CE), are provided in the supporting information.

Two statistical methods were used to identify characteristic compositions in the AMS mass fragment spectra. Positive Matrix Factorization (PMF) incorporates weighting of residuals from factorization by measurement

errors [*Paatero*, 1997; *Paatero and Tapper*, 1994; *Paatero and Hopke*, 2003; *Paatero et al.*, 2002] and has been widely used for atmospheric source apportionment [*Reff et al.*, 2007; *Weber et al.*, 2007]. AMS PMF factors associate mixtures of organic aerosol components to specific emission sources [*Jimenez et al.*, 2009; *Lanz et al.*, 2007; *Ulbrich et al.*, 2009]. K-means clustering aims to partition observations into clusters in which each observation belongs to the cluster with the nearest mean [*Hartley*, 1955]. K-means clustering has been applied to AMS light scattering single-particle spectra to identify atmospheric particle types [*Lee et al.*, 2015, 2016a; *Liu et al.*, 2013; *Willis et al.*, 2016]. The criteria used for identifying the most accurate and robust solutions for both PMF and K-means clustering are provided in the supporting information.

Three factors were identified by PMF of the AMS high-resolution measurements: Factor44 (vehicle-related SOA) with a high fraction of oxygenated organic mass fragment ions (including *m/z* 44), Factor82 (sulfate-related bSOA) with high *m/z* 82 ion signals (IEPOX-OA), and Factor91 (nitrate-related bSOA) with high *m/z* 91 ion signals. K-means clustering of LS mode single-particle measurements also identified three types of particles: Cluster44 with a high fraction of oxidized organic fragment ions at *m/z* 43 and 44, Cluster82 with a high sulfate fraction and *m/z* 82 fragment ion signals, and Cluster91 with a high fraction of less oxidized organic mass fragment ions (including *m/z* 91). Interestingly, although the clusters were based on single-particle measurements while factors were from mass-based measurements, they resulted in very similar mass spectra, as indicated by the near-unity values of the cosine similarity between the *m/z* spectra and moderate to strong correlations of the time series (shown in Table S5). The correlation of the time series of the concentrations of Factor82 mass and Cluster82 number was $r = 0.80$, which was higher than that of Factor44 and Cluster44 ($r = 0.66$) and of Factor91 and Cluster91 ($r = 0.48$).

3. Aerosol Observations at Look Rock, TN

Figure 1 summarizes the AMS organic aerosol mass concentrations observed at Look Rock during SOAS. The AMS CE-corrected concentration of nonrefractory submicron particle mass was 5.3 $\mu g\ m^{-3}$, with 66% organic components followed by 22% sulfate fragments. Ammonium accounted for 8% of mass, and nitrate (1%) and chloride (0.2%) were consistently low (Figure 1). Black carbon (BC) measured by aethelometer made up 4% of the submicron mass, as described by *Budisulistiorini et al.* [2015]. Dust [*Usher et al.*, 2003] was 3% of submicron mass for the 17 of 47 days for which X-ray fluorescence was available, as described in the supporting information. The meteorological, biological, and chemical factors that contribute to these aerosol concentrations are evaluated below.

3.1. Enhancement of Particle Concentrations by Stagnation

One interesting feature of the AMS submicron particle mass concentration time series is that multiple-day events of nearly continuously increasing concentrations are much more evident than diurnal cycles. Each event consists of 3–6 days of concentrations higher than 2 $\mu g\ m^{-3}$, typically ended by a rain event that scavenged most of the aerosol mass. Dividing the campaign according to these criteria shows that there are seven multiday periods of aerosol accumulation that are separated by low AMS organic concentration during the 7 week campaign (Figure 1).

Most of these events are characterized by 3–4 days of continually increasing concentration that obscure the midday peaks expected for daytime production of photochemical SOA. To illustrate the photochemical contribution to SOA, we calculated the loading in the boundary layer column, assuming a well-mixed boundary layer source and negligible concentrations above the layer [*Wagner et al.*, 2015] (details in the supporting information) with regional soundings and reanalyses for mixed layer height (Figure S7) [*Draxier and Hess*, 1998; *Wang and Wang*, 2014]. Figure 2 shows the daytime loading in the boundary layer column (defined as from 0900 to 2100) accounted for 92% of the daily loading in the boundary layer column for nonrefractory organic components for the 48 day campaign. The diurnal cycles of the three PMF factors are similar to that of the combined nonrefractory organic components. Higher isoprene concentrations were moderately correlated ($r = 0.68$) to higher daily maximum radiation, which likely contributed to part of the multiday event pattern by contributing more SOA on days with fewer clouds.

Other causes of the high-OM events likely include the low wind conditions associated with all seven events, suggesting that stagnation might be contributing to the high aerosol concentration events (Figure S9). The frequencies of occurrence of the highest concentrations of OM and all three factors are higher at lower wind

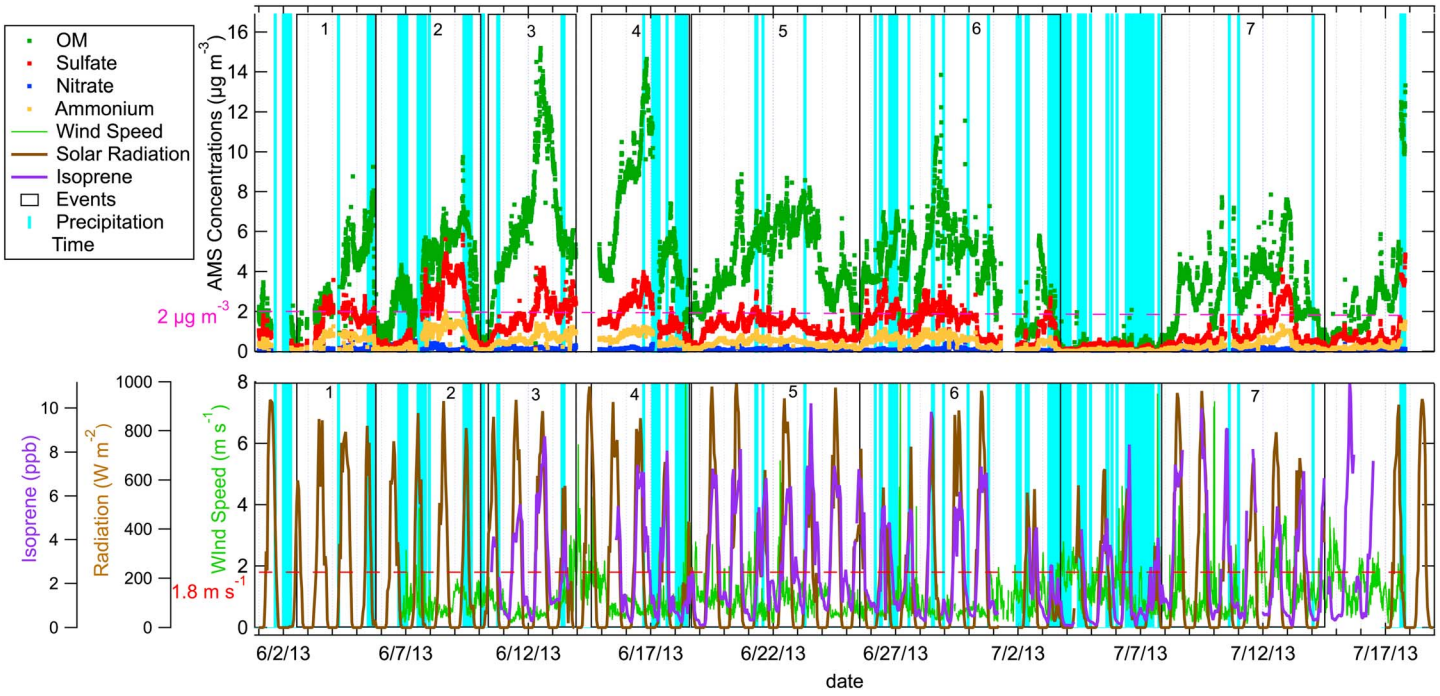

Figure 1. (top) Time series of AMS nonrefractory submicron mass concentrations of OM, sulfate, nitrate, and ammonium (2 μg m^{-3} OM is marked on the plot to indicate the criterion for separation between the seven events identified). (bottom) Time series of isoprene concentration, solar radiation, precipitation, and wind speed (1.8 m s^{-1} is marked on the plot as a cutoff for low wind speed associated with stagnation conditions).

speeds, in particular at less than 1.8 m s^{-1}. The seven high-OM events are not associated with back trajectories from a particular region, indicating that a single location of emission sources (power plant or forest) does not explain the pattern of events, as shown in Figure S5.

3.2. Comparison of Mass-Based AMS Factor and Number-Based LS Cluster Sources

By comparing the AMS PMF factor mass spectra to factors reported in the literature and by evaluating the correlations of time series of factor concentrations to tracers, the probable source of each factor was identified. Factor44 and Cluster44 had moderate correlations with several anthropogenic emission tracers ($r > 0.5$ for BC, CO, NO_y, and O_3) and had clear diurnal cycles that peaked for about 3 h after local noon each day, similar to the results of *Q. Zhang et al.* [2011]. The moderate correlation ($r = 0.73$ and 0.58, respectively) of both Factor44 and Cluster44 time series to BC concentration time series (shown in Figure 3) suggests that the

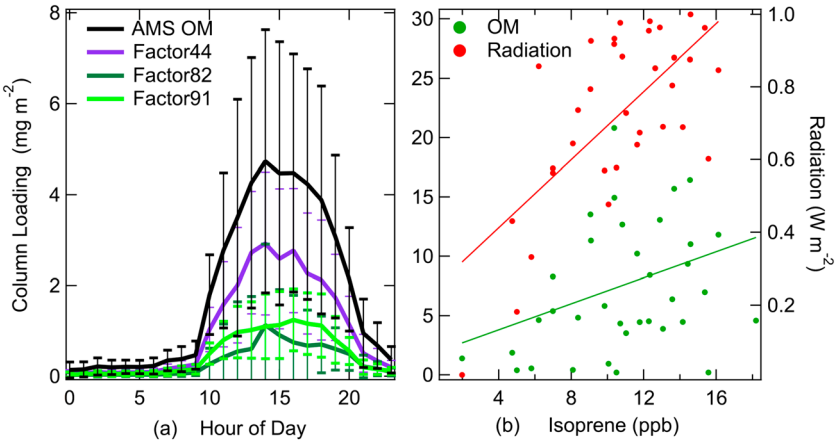

Figure 2. (a) Diurnal pattern of loading in the boundary layer column of the three PMF factors. Errors bars give the standard deviation to indicate variability. (b) Comparison of organic loading in the boundary layer column and maximum daily solar radiation (400 to 1100 nm wavelength) with isoprene ($R = 0.32$ and 0.68, respectively).

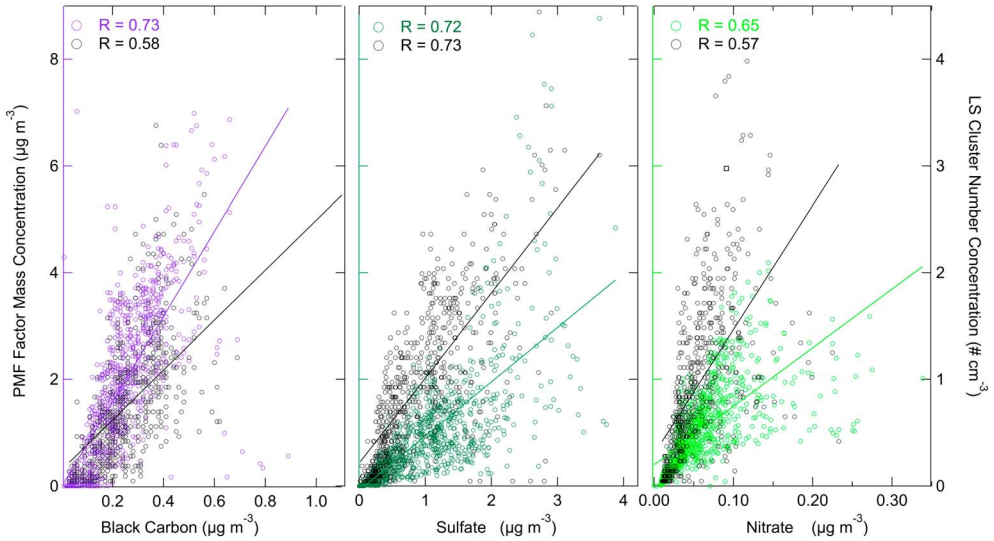

Figure 3. Hourly averaged scatterplots of AMS HR PMF factors and LS-AMS clusters with tracers for anthropogenic emissions: (left) Factor44 and Cluster44 versus Black Carbon (BC), r = 0.73 and 0.58, respectively; (middle) Factor82 and Cluster82 versus sulfate, r = 0.72 and 0.73, respectively; and (right) Factor91 and Cluster91 versus nitrate, r = 0.65 and 0.57, respectively. Normalized hourly averaged concentration is shown in the plots; lines are the linear regression of factors and clusters. Only hours for which the LS-detectable range (230 < mobility diameter < 500 nm, measured by SEMS) represented more than 50% of submicron mass were included in this correlation, which was approximately 87% of the 33 day study.

factor is influenced by aged anthropogenic combustion emissions from regional vehicle traffic emissions. Factor44 also showed moderate correlations to sulfate (r = 0.76) and nitrate (r = 0.63), consistent with transported and aged OM typically from anthropogenic emissions [*Jimenez et al.*, 2009]. The afternoon maximum indicated that photochemical reactions likely caused the aerosol formation. Factor44 was similar to AMS spectra of gasoline and diesel SOA in a region with high *m/z* 44 fraction (~0.1) and low *m/z* 43 fraction (~0.05) [*Presto et al.*, 2014] and to their ambient LV-OOA factor, which was attributed to vehicle sources (see also in Text S2) [*Elsasser et al.*, 2012; *Fine et al.*, 2001; *Mano and Andreae*, 1994].

Factor82 and Cluster82 were moderately correlated (r = 0.72 and 0.73, respectively) with sulfate concentration time series, as given in Figure 3. This correlation suggests that Factor82 and Cluster82 are likely from acid-catalyzed reactive uptake of IEPOX that occurred in the presence of acidic sulfate, consistent with previous studies [*Lin et al.*, 2012; *Surratt et al.*, 2010]. Factor91 and Cluster91 time series were moderately correlated (r = 0.65 and 0.57, respectively) with nitrate concentration, which can indicate several types of combustion and oxidants [*Song et al.*, 2001] as well as N_2O_5 reactive uptake [*Finlayson-Pitts et al.*, 1989]. Isoprene concentration (~2 ppb) is higher than monoterpene (<1 ppb) during the SOAS study [*Budisulistiorini et al.*, 2015]. Factor91 had a maximum concentration at 1300 (Figure S10). Both of these features are more consistent with isoprene as a source of Factor91 since isoprene concentration had a strong correlation (r = 0.83) to the measured radiation at the surface. Therefore, Factor91 is likely to also be formed from isoprene through a non-IEPOX route based on the similarity to published mass spectra from smog chamber products of isoprene oxidized under relatively low-sulfate and NO_x conditions [*Budisulistiorini et al.*, 2016; *Chen et al.*, 2015; *Liu et al.*, 2016; *Riva et al.*, 2016]. Factor91 could also be from a number of other sources, given the many associations of this marker fragment reported previously (Table S4). Factor91 is similar to a previously reported OOA3 PMF factor in *Chen et al.* [2015] with cosine similarity of 0.87, which was adequately reconstructed by a linear combination of multiple lab-generated bSOA (30% α-pinene-derived OM, 20% β-caryophyllene-derived OM, and 50% isoprene-derived OM). Organic nitrate has also been calculated in this study with the NO^+/NO_2^+ ratio method [*Xu et al.*, 2015a], as described in Text S5. The estimated fraction of molecules containing organonitrate groups (3.2–16.4% of OM) is comparable with *Xu et al.* [2015a] (5–12%) and could indicate a potential connection between organic nitrate and Factor91. However, there were no nighttime increases of Factor91, NO_x, or nitrate (Figure S10), which rules out a contribution to Factor91 from nighttime monoterpene-NO_x reactions. In addition, the weak correlation (r = 0.48) of the

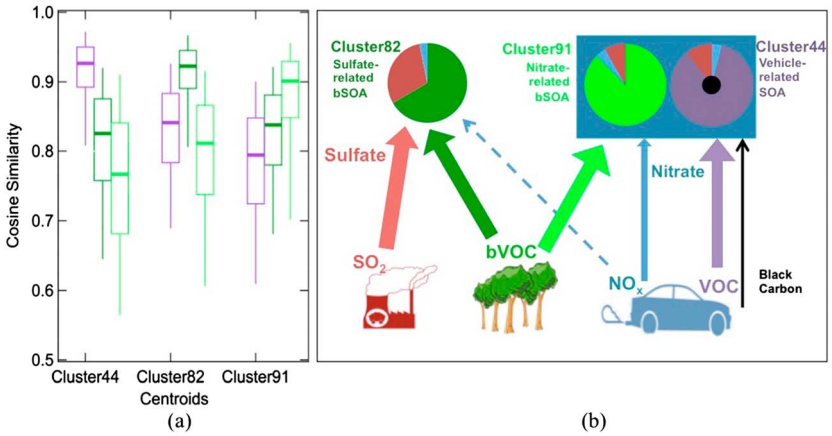

Figure 4. (a) Cosine similarity of individual single-particle LS-AMS mass spectra to the centroids of the three clusters. Purple: cluster44, 9808 particles; dark green: cluster82; 12022 particles; light green: cluster 91, 12598 particles. The boxes show the 25th and 75th percentile values; the Whiskers show the 5th and 95th percentile values. (b) Schematic diagram of sources, processes, and final mixing state of aerosols in Look Rook, Tennessee, for summer 2013. The particle pie graphs are proportional to the nonrefractory signal fractions of the three Clusters (ammonium is excluded because of baseline noise in LS spectra [*Lee et al.*, 2015], and chloride is excluded because it is negligible). The processes shown are based on both direct measurements and correlations.

time series of Factor91 and Cluster91 and the similar fractions of nitrate on all three particle types (26%, 37%, and 39% of nitrate were on Cluster44, Cluster82, and Cluster91, respectively) indicate that Factor91 was not forming selectively on Cluster91 particles.

3.3. Evidence for Selective Formation of *m/z* 82 Factor and Sulfate-Containing Particles

To investigate the dependence of the clustering of the organic mass fragment ions on the inorganic components, K-means clustering was carried out with only organic mass fragment ions and with all nonrefractory mass fragment ions. The two clustering approaches produced nearly identical groups of particles, and this high degree of consistency shows that the method was robust in producing similar particle types with or without inorganic components. In addition, spectra within each cluster were very similar to the spectrum of the centroid for that cluster. The distributions of cosine similarities of the individual particles and the cluster centroid spectra in Figure 4a show that all of the spectra in each cluster were both well separated from other clusters and very similar to the centroid spectrum.

The robustness and separation of the clusters show that the particles are externally mixed, namely that the three distinct types of particles have different compositions. The strong association of Factor82 with bSOA on Cluster82 particles that contain sulfate from power plants (time series correlation of $r = 0.80$ and cosine similarity of mass spectra of 0.97) indicates that partitioning of IEPOX to particles was likely chemically selective. More than 76% of the sulfate ion signal is in Cluster82, and the sulfate signal fraction is 0.17 for Cluster82 but less than 0.08 for the other two clusters. This difference is shown in Figure S8. This preference for Factor82 condensing onto particular particles could be driven by reactive uptake caused by sulfate, acidity, or other components [*Gaston et al.*, 2014a; *Lin et al.*, 2012; *Riedel et al.*, 2015; *Surratt et al.*, 2010, *Surratt et al.*, 2006], but the correlation to sulfate indicates that sulfate is likely a controlling reactant. In addition, potential organosulfate group concentrations measured by FTIR correlated moderately with Factor82 ($r = 0.69$), providing a direct role for sulfate in the particle-phase reactions. The organosulfate is likely related to the IEPOX-derived organosulfates that were previously reported at Look Rock to be the most abundant organosulfates [*Budisulistiorini et al.*, 2015], further showing that particle-phase reactions of IEPOX with sulfate may have been the reactions that effectively pulled the gas-to-particle equilibrium toward the particle phase. In contrast, the inorganic components from Cluster44 and Cluster91 are very similar to each other, and Factor91 is not as strongly correlated to Cluster91 (Table S5), meaning that production pathways of the "vehicle-related SOA" and the "nitrate-related bSOA" are, in contrast, independent of inorganic particle composition and hence likely limited by gas-phase reactions. Figure 4b shows a schematic diagram of the sources, processes, and resulting mixture of aerosol particle types that are consistent with these observations.

The timing of emissions from collocated sources could also have contributed to the separation of the factors onto different particles and may explain the association of Factor44 with Cluster44 ($r = 0.66$) and BC ($r = 0.73$) since vehicles emit both BC and Factor44 precursors. However, the correlation of Factor82 (isoprene related) bSOA with (anthropogenic) sulfate ($r = 0.72$) and organosulfate ($r = 0.69$) cannot be explained by collocation.

4. Conclusions

Stagnation events at lower wind speeds were an important factor controlling day-to-day changes in aerosol concentration at Look Rock during SOAS, masking the typical diurnal pattern expected for secondary photochemical aerosol. However, aerosol loading in the boundary layer column from scaling concentrations by reanalysis estimates of boundary layer height showed a peak in the afternoon for all factors and clusters that correlated to solar radiation and isoprene concentration, consistent with sunlight-driven reactions. Daytime loading in the boundary layer column of organic aerosols is estimated to account for 92% of the daily column loading during the campaign, consistent with the expectation that photochemical reaction is the likely mechanism for most of the secondary aerosol formation at the site.

The similarity of the three types of single particles and the three mass-based factors as well as the significant differences between the particle types suggest that the aerosol particles were largely separated into three distinct types of organic particles. The most oxidized organic aerosol type and factor (Factor44 and Cluster44) were from (at least in part) vehicle-related sources and accounted for 42% of particle mass and 28% of particle number. The "sulfate-related" bSOA Factor82 and Cluster82 were similar to factors identified previously as produced from isoprene oxidation under low-NO pathways in the presence of acidic sulfate aerosol [*Budisulistiorini et al.*, 2013, 2015; *Xu et al.*, 2015b] and accounted for 20% of the mass and 35% of the number of the measured aerosol. The "nitrate-related" bSOA (Factor91 and Cluster91) had similar time series correlation to nitrate concentration as Factor44 and similar nitrate fraction as Cluster 44 and accounted for 34% of mass and 37% of number of the measured aerosol.

The strong time series correlation ($r = 0.80$) of the mass-based Factor82 and the number-based Cluster82 as well as the distinct differences between the three particle types provides the most direct single-particle composition evidence to date of the selective uptake of biogenic volatile organic compound oxidation products onto particles containing (anthropogenic) sulfate. Since the Cluster82 particle type has 76% of the sulfate on all clusters of the detected single particle size range, this correlation and composition provide a strong indication that particle-phase reactions of isoprene-derived oxidation products with sulfate were responsible for Factor82. This pathway is also consistent with the moderate correlation ($r = 0.69$) between Factor82 and organosulfate groups and fragments as well as with laboratory identification of organosulfate formation pathways [*Budisulistiorini et al.*, 2015; *Surratt et al.*, 2010]. In contrast, the moderate correlation ($r = 0.65$) of nitrate with "nitrate-related" bSOA (Factor91) and the weak correlation of Factor91 with Cluster91 ($r = 0.48$), as well as the lower nitrate signal (39%) on Cluster91 than sulfate signal (76%) on Cluster82, mean that composition-dependent particle-phase reactions likely did not contribute to Factor91 bSOA.

The similarity and correlation of the mass and single-particle chemical compositions provide the first direct evidence of selective uptake of isoprene-related bSOA onto sulfate-containing particles. These results show the significance of heterogeneous reactions on sulfate particles from anthropogenic emissions for bSOA and specifically link the near doubling of bSOA to sulfate from power plants in the region. Recent studies have shown that hygroscopicity [*Cerully et al.*, 2015] and optical properties [*Washenfelder et al.*, 2015] are related to different PMF factors of organic aerosols in the southeastern U.S. Combining these findings with the identification of the three distinct particle types in this study implies that the optical and drop-nucleating properties of each particle type may be different from those of other types. For this reason, future work linking the chemical characterization of particle types to their different properties explicitly would improve constraints on the direct and indirect radiative forcing of particles in the southeastern U.S.

Acknowledgments
We thank Ashley Corrigan, Janin Guzman-Morales, Katie Kolesar, Xiaolu Zhang, Chris Cappa, and Timothy H. Bertram for assistance at the field site. The authors thank Annmarie Carlton, Joost deGouw, Jose Jimenez, and Allen Goldstein for organizing the SOAS campaign and Sherri Hunt for supporting this project. This work was supported by U.S. Environmental Protection Agency grant RD-83540801. This work has not been formally reviewed by the EPA. The views expressed in this document are solely those of the authors, and the EPA does not endorse any products or commercial services mentioned in this publication. The measurements used in this study are curated at http://doi.org/10.6075/J0P26W1T and are available at the project archive http://esrl.noaa.gov/csd/groups/csd7/measurements/2013senex/Ground/DataDownload.

References

Banerjee, A., L. M. Polvani, and J. C. Fyfe (2017), The United States "warming hole": Quantifying the forced aerosol response given large internal variability, *Geophys. Res. Lett.*, *44*, 1928–1937, doi:10.1002/2016GL071567.

Bates, T. S., et al. (2012), Measurements of ocean derived aerosol off the coast of California, *J. Geophys.*, *117*, D00V15, doi:10.1029/2012JD017588.

Boyd, C. M., J. Sanchez, L. Xu, A. J. Eugene, T. Nah, W. Y. Tuet, M. I. Guzman, and N. L. Ng (2015), Secondary organic aerosol formation from the beta-pinene+NO_3 system: Effect of humidity and peroxy radical fate, *Atmos. Chem. Phys.*, *15*(13), 7497–7522.

Budisulistiorini, S. H., et al. (2013), Real-time continuous characterization of secondary organic aerosol derived from isoprene epoxydiols in downtown Atlanta, Georgia, using the aerodyne aerosol chemical speciation monitor, *Environ. Sci. Technol.*, *47*(11), 5686–5694.

Budisulistiorini, S. H., et al. (2015), Examining the effects of anthropogenic emissions on isoprene-derived secondary organic aerosol formation during the 2013 southern oxidant and aerosol study (SOAS) at the look rock, Tennessee ground site, *Atmos. Chem. Phys.*, *15*(15), 8871–8888.

Budisulistiorini, S. H., K. Baumann, E. S. Edgerton, S. T. Bairai, S. Mueller, S. L. Shaw, E. M. Knipping, A. Gold, and J. D. Surratt (2016), Seasonal characterization of submicron aerosol chemical composition and organic aerosol sources in the southeastern United States: Atlanta, Georgia,and Look Rock, Tennessee, *Atmos. Chem. Phys.*, *16*(8), 5171–5189.

Cerully, K. M., A. Bougiatioti, J. R. Hite, H. Guo, L. Xu, N. L. Ng, R. Weber, and A. Nenes (2015), On the link between hygroscopicity, volatility, and oxidation state of ambient and water-soluble aerosols in the southeastern United States, *Atmos. Chem. Phys.*, *15*(15), 8679–8694.

Chen, Q., et al. (2015), Submicron particle mass concentrations and sources in the Amazonian wet season (AMAZE-08), *Atmos. Chem. Phys.*, *15*(7), 3687–3701.

Corrigan, A. L., et al. (2013), Biogenic and biomass burning organic aerosol in a boreal forest at Hyytiälä, Finland, during HUMPPA-COPEC 2010, *Atmos. Chem. Phys.*, *13*(24), 12,233–12,256.

Cross, E. S., J. G. Slowik, P. Davidovits, J. D. Allan, D. R. Worsnop, J. T. Jayne, D. K. Lewis, M. Canagaratna, and T. B. Onasch (2007), Laboratory and ambient particle density determinations using light scattering in conjunction with aerosol mass spectrometry, *Aerosol Sci. Technol.*, *41*(4), 343–359.

Cross, E. S., T. B. Onasch, M. Canagaratna, J. T. Jayne, J. Kimmel, X. Y. Yu, M. L. Alexander, D. R. Worsnop, and P. Davidovits (2009), Single particle characterization using a light scattering module coupled to a time-of-flight aerosol mass spectrometer, *Atmos. Chem. Phys.*, *9*(20), 7769–7793.

Devore, J. L., and K. N. Berk (2012), *Modern Mathematical Statistics with Application*, 2nd ed., Springer Science+Business Media, LLC, New York.

Draxier, R. R., and G. D. Hess (1998), An overview of the HYSPLIT_4 modelling system for trajectories, dispersion and deposition, *Aust. Meteorol. Mag.*, *47*(4), 295–308.

Elsasser, M., et al. (2012), Organic molecular markers and signature from wood combustion particles in winter ambient aerosols: Aerosol mass spectrometer (AMS) and high time-resolved GC-MS measurements in Augsburg, Germany, *Atmos. Chem. Phys.*, *12*(14), 6113–6128.

Fine, P. M., G. R. Cass, and B. R. T. Simoneit (2001), Chemical characterization of fine particle emissions from fireplace combustion of woods grown in the northeastern United States, *Environ. Sci. Technol.*, *35*(13), 2665–2675.

Finlayson-Pitts, B. J., M. J. Ezell, and J. N. Pitts (1989), Formation of chemically active chlorine compounds by reactions of atmospheric NaCl particles with gaseous N_2O_5 and $ClONO_2$, *Nature*, *337*(6204), 241–244.

Ford, B., and C. L. Heald (2013), Aerosol loading in the southeastern United States: Reconciling surface and satellite observations, *Atmos. Chem. Phys.*, *13*(18), 9269–9283.

Gaston, T., P. Riedel, Z. F. Zhang, A. Gold, J. D. Surratt, and J. A. Thornton (2014a), Reactive uptake of an isoprene-derived epoxydiol to submicron aerosol particles, *Environ. Sci. Technol.*, *48*(19), 11178–11186.

Gaston, T., P. Riedel, Z. F. Zhang, A. Gold, J. D. Surratt, and J. A. Thornton (2014b), Reactive uptake of an isoprene-derived epoxydiol to submicron aerosol particles, *Environ. Sci. Technol.*, *48*(19), 11178–11186.

Goldstein, A. H., C. D. Koven, C. L. Heald, and I. Y. Fung (2009), Biogenic carbon and anthropogenic pollutants combine to form a cooling haze over the southeastern United States, *Proc. Natl. Acad. Sci. U.S.A.*, *106*(22), 8835–8840.

Guenther, X., C. Jiang, L. Heald, T. Sakulyanontvittaya, T. Duhl, L. K. Emmons, and X. Wang (2012), The model of emissions of gases and aerosols from nature version 2.1 (MEGAN2.1): An extended and updated framework for modeling biogenic emissions, *Geosci. Model Dev.*, *5*(6), 1471–1492.

Hallquist, M., et al. (2009), The formation, properties and impact of secondary organic aerosol: Current and emerging issues, *Atmos. Chem. Phys.*, *9*(14), 5155–5236.

Hartley, H. O. (1955), Some recent developments in analysis of variance, *Commun. Pure Appl. Math.*, *8*(1), 47–72.

Hu, W. W., et al. (2016), Volatility and lifetime against OH heterogeneous reaction of ambient isoprene-epoxydiols-derived secondary organic aerosol (IEPOX-SOA), *Atmos. Chem. Phys.*, *16*(18), 11563–11580.

Jimenez, J. L., et al. (2009), Evolution of organic aerosols in the atmosphere, *Science*, *326*(5959), 1525–1529.

Kim, P. S., et al. (2015), Sources, seasonality, and trends of southeast US aerosol: An integrated analysis of surface, aircraft, and satellite observations with the GEOS-Chem chemical transport model, *Atmos. Chem. Phys.*, *15*(18), 10411–10433.

Kostenidou, E., R. K. Pathak, and S. N. Pandis (2007), An algorithm for the calculation of secondary organic aerosol density combining AMS and SMPS data, *Aerosol Sci. Technol.*, *41*(11), 1002–1010.

Krechmer, J. E., et al. (2015), Formation of low volatility organic compounds and secondary organic aerosol from isoprene hydroxyhydroperoxide low-NO oxidation, *Environ. Sci. Technol.*, *49*(17), 10,330–10,339.

Lanz, V. A., M. R. Alfarra, U. Baltensperger, B. Buchmann, C. Hueglin, and A. S. H. Prevot (2007), Source apportionment of submicron organic aerosols at an urban site by factor analytical modelling of aerosol mass spectra, *Atmos. Chem. Phys.*, *7*(6), 1503–1522.

Lee, A. K. Y., M. D. Willis, R. M. Healy, T. B. Onasch, and J. P. D. Abbatt (2015), Mixing state of carbonaceous aerosol in an urban environment: Single particle characterization using the soot particle aerosol mass spectrometer (SP-AMS), *Atmos. Chem. Phys.*, *15*(4), 1823–1841.

Lee, A. K. Y., M. D. Willis, R. M. Healy, J. M. Wang, C. H. Jeong, J. C. Wenger, G. J. Evans, and J. P. D. Abbatt (2016a), Single-particle characterization of biomass burning organic aerosol (BBOA): Evidence for non-uniform mixing of high molecular weight organics and potassium, *Atmos. Chem. Phys.*, *16*(9), 5561–5572.

Lee, A. K. Y., J. P. D. Abbatt, W. R. Leaitch, S. M. Li, S. J. Sjostedt, J. J. B. Wentzell, J. Liggio, and A. M. Macdonald (2016b), Substantial secondary organic aerosol formation in a coniferous forest: Observations of both day- and nighttime chemistry, *Atmos. Chem. Phys.*, *16*(11), 6721–6733.

Lin, Y.-H., et al. (2012), Isoprene epoxydiols as precursors to secondary organic aerosol formation: Acid-catalyzed reactive uptake studies with authentic compounds, *Environ. Sci. Technol.*, *46*(1), 250–258.

Liu, J. M., et al. (2016), Efficient isoprene secondary organic aerosol formation from a non-IEPDX pathway, *Environ. Sci. Technol.*, *50*(18), 9872–9880.

Liu, S., L. M. Russell, D. T. Sueper, and T. B. Onasch (2013), Organic particle types by single-particle measurements using a time-of-flight aerosol mass spectrometer coupled with a light scattering module, *Atmos. Meas. Tech.*, *6*(2), 187–197.

Mano, S., and M. O. Andreae (1994), Emission of methyl-bromide from biomass burning, *Science*, *263*(5151), 1255–1257.

Nguyen, T. B., P. J. Roach, J. Laskin, A. Laskin, and S. A. Nizkorodov (2011), Effect of humidity on the composition of isoprene photooxidation secondary organic aerosol, *Atmos. Chem. Phys.*, *11*(14), 6931–6944.
Nguyen, T. B., et al. (2015), Mechanism of the hydroxyl radical oxidation of methacryloyl peroxynitrate (MPAN) and its pathway toward secondary organic aerosol formation in the atmosphere, *Phys. Chem. Chem. Phys.*, *17*(27), 17914–17926.
Nguyen, T. K. V., V. P. Ghate, and A. G. Carlton (2016), Reconciling satellite aerosol optical thickness and surface fine particle mass through aerosol liquid water, *Geophys. Res. Lett.*, *43*, 11,903–11,912, doi:10.1002/2016GL070994.
Paatero, P. (1997), Least squares formulation of robust non-negative factor analysis, *Chemom. Intell. Lab. Syst.*, *37*(1), 23–35.
Paatero, P., and P. K. Hopke (2003), Discarding or downweighting high-noise variables in factor analytic models, *Anal. Chim. Acta*, *490*(1–2), 277–289.
Paatero, P., and U. Tapper (1994), Positive matrix factorization: A non-negative factor model with optimal utilization of error estimates of data values, *Environmetrics*, *5*(2), 111–126.
Paatero, P., P. K. Hopke, X. H. Song, and Z. Ramadan (2002), Understanding and controlling rotations in factor analytic models, *Chemom. Intell. Lab. Syst.*, *60*(1–2), 253–264.
Portmann, R. W., S. Solomon, and G. C. Hegerl (2009), Spatial and seasonal patterns in climate change, temperatures, and precipitation across the United States, *Proc. Natl. Acad. Sci. U.S.A.*, *106*(18), 7324–7329.
Presto, A. A., T. D. Gordon, and A. L. Robinson (2014), Primary to secondary organic aerosol: Evolution of organic emissions from mobile combustion sources, *Atmos. Chem. Phys.*, *14*(10), 5015–5036.
Rattanavaraha, W., et al. (2016), Assessing the impact of anthropogenic pollution on isoprene-derived secondary organic aerosol formation in PM2.5 collected from the Birmingham, Alabama, ground site during the 2013 southern oxidant and aerosol study, *Atmos. Chem. Phys.*, *16*(8), 4897–4914.
Reff, A., S. I. Eberly, and P. V. Bhave (2007), Receptor modeling of ambient particulate matter data using positive matrix factorization: Review of existing methods, *J. Air Waste Manage. Assoc.*, *57*(2), 146–154.
Riedel, T. P., Y.-H. Lin, H. Budisulistiorini, C. J. Gaston, J. A. Thornton, Z. Zhang, W. Vizuete, A. Gold, and J. D. Surrattt (2015), Heterogeneous reactions of isoprene-derived epoxides: Reaction probabilities and molar secondary organic aerosol yield estimates, *Environ. Sci. Technol. Lett.*, *2*(2), 38–42.
Rinne, H. J. I., A. B. Guenther, J. P. Greenberg, and P. C. Harley (2002), Isoprene and monoterpene fluxes measured above Amazonian rainforest and their dependence on light and temperature, *Atmos. Environ.*, *36*(14), 2421–2426.
Riva, M., et al. (2016), Chemical characterization of secondary organic aerosol from oxidation of isoprene hydroxyhydroperoxides, *Environ. Sci. Technol.*, *50*(18), 9889–9899.
Robinson, N. H., et al. (2011), Evidence for a significant proportion of secondary organic aerosol from isoprene above a maritime tropical forest, *Atmos. Chem. Phys.*, *11*(3), 1039–1050.
Russell, L. M., R. Bahadur, L. N. Hawkins, J. Allan, D. Baumgardner, P. K. Quinn, and T. S. Bates (2009), Organic aerosol characterization by complementary measurements of chemical bonds and molecular fragments, *Atmos. Environ.*, *43*(38), 6100–6105.
Slowik, J. G., et al. (2011), Photochemical processing of organic aerosol at nearby continental sites: Contrast between urban plumes and regional aerosol, *Atmos. Chem. Phys.*, *11*(6), 2991–3006.
Song, X. H., A. V. Polissar, and P. K. Hopke (2001), Sources of fine particle composition in the northeastern US, *Atmos. Environ.*, *35*(31), 5277–5286.
Surratt, J. D., et al. (2006), Chemical composition of secondary organic aerosol formed from the photooxidation of isoprene, *J. Phys. Chem. A*, *110*(31), 9665–9690.
Surratt, J. D., A. W. H. Chan, N. C. Eddingsaas, M. Chan, C. L. Loza, A. J. Kwan, S. P. Hersey, R. C. Flagan, P. O. Wennberg, and J. H. Seinfeld (2010), Reactive intermediates revealed in secondary organic aerosol formation from isoprene, *Proc. Natl. Acad. Sci. U.S.A.*, *107*(15), 6640–6645.
Takahama, S., A. Johnson, and L. M. Russell (2013), Quantification of carboxylic and carbonyl functional groups in organic aerosol infrared absorbance spectra, *Aerosol Sci. Technol.*, *47*(3), 310–325.
Ulbrich, I. M., M. R. Canagaratna, Q. Zhang, D. R. Worsnop, and J. L. Jimenez (2009), Interpretation of organic components from positive matrix factorization of aerosol mass spectrometric data, *Atmos. Chem. Phys.*, *9*(9), 2891–2918.
Usher, C. R., A. E. Michel, and V. H. Grassian (2003), Reactions on mineral dust, *Chem. Rev.*, *103*(12), 4883–4939.
Wagner, N. L., et al. (2015), In situ vertical profiles of aerosol extinction, mass, and composition over the southeast United States during SENEX and SEAC^{4}RS: Observations of a modest aerosol enhancement aloft, *Atmos. Chem. Phys.*, *15*(12), 7085–7102.
Wang, X. Y., and K. C. Wang (2014), Estimation of atmospheric mixing layer height from radiosonde, *Atmos. Meas. Tech.*, *7*(6), 1701–1709.
Washenfelder, R. A., et al. (2015), Biomass burning dominates brown carbon absorption in the rural southeastern United States, *Geophys. Res. Lett.*, *42*, 653–664, doi:10.1002/2014GL062444.
Weber, R. J., et al. (2007), A study of secondary organic aerosol formation in the anthropogenic-influenced southeastern United States, *J. Geophys. Res.*, *112*, D13302, doi:10.1029/2007JD008408.
Willis, M. D., R. M. Healy, N. Riemer, M. West, J. M. Wang, C. H. Jeong, J. C. Wenger, G. J. Evans, J. P. D. Abbatt, and A. K. Y. Lee (2016), Quantification of black carbon mixing state from traffic: Implications for aerosol optical properties, *Atmos. Chem. Phys.*, *16*(7), 4693–4706.
Worton, D. R., et al. (2013), Observational insights into aerosol formation from isoprene, *Environ. Sci. Technol.*, *47*(20), 11403–11413.
Xu, L., S. Suresh, H. Guo, R. J. Weber, and N. L. Ng (2015a), Aerosol characterization over the southeastern United States using high-resolution aerosol mass spectrometry: Spatial and seasonal variation of aerosol composition and sources with a focus on organic nitrates, *Atmos. Chem. Phys.*, *15*(13), 7307–7336.
Xu, L., et al. (2015b), Effects of anthropogenic emissions on aerosol formation from isoprene and monoterpenes in the southeastern United States, *Proc. Natl. Acad. Sci. U.S.A.*, *112*(1), 37–42.
Xu, L., et al. (2016), Enhanced formation of isoprene-derived organic aerosol in sulfur-rich power plant plumes during Southeast Nexus, *J. Geophys. Res. Atmos.*, *121*, 11,137–11,153, doi:10.1002/2016JD025156.
Yu, S. C., K. Alapaty, R. Mathur, J. Pleim, Y. H. Zhang, C. Nolte, B. Eder, K. Foley, and T. Nagashima (2014), Attribution of the United States "warming hole": Aerosol indirect effect and precipitable water vapor, *Sci. Rep.*, *4*, 10, doi:10.1038/srep06929.
Zhang, H., J. D. Surratt, Y. H. Lin, J. Bapat, and R. M. Kamens (2011), Effect of relative humidity on SOA formation from isoprene/NO photooxidation: Enhancement of 2-methylglyceric acid and its corresponding oligoesters under dry conditions, *Atmos. Chem. Phys.*, *11*(13), 6411–6424.
Zhang, Q., J. L. Jimenez, M. R. Canagaratna, I. M. Ulbrich, N. L. Ng, D. R. Worsnop, and Y. L. Sun (2011), Understanding atmospheric organic aerosols via factor analysis of aerosol mass spectrometry: A review, *Anal. Bioanal. Chem.*, *401*(10), 3045–3067.